1521-009X/43/11/1795–1804$25.00
Drug Metabolism and Disposition
Copyright © 2015 by The American Society for Pharmacology and Experimental Therapeutics
http://dx.doi.org/10.1124/dmd.114.058685
Drug Metab Dispos 43:1795–1804, November 2015

Modulation of P-glycoprotein at the Human Blood-Brain Barrier by Quinidine or Rifampin Treatment: A Positron Emission Tomography Imaging Study

Li Liu, Ann C. Collier, Jeanne M. Link, Karen B. Domino, David A. Mankoff, Janet F. Eary, Charles F. Spiekerman, Peng Hsiao, Anand K. Deo, and Jashvant D. Unadkat

Department of Pharmaceutics (L.L., P.H., A.K.D., J.D.U.), Department of Medicine (A.C.C.), Division of Nuclear Medicine (J.M.L., D.A.M., J.F.E.), Department of Anesthesiology and Pain Medicine (K.B.D.), and Department of Oral Health Sciences (C.F.S.), University of Washington, Seattle, Washington

Received May 14, 2014; accepted September 1, 2015

ABSTRACT

Permeability-glycoprotein (P-glycoprotein, P-gp), an efflux transporter at the human blood-brain barrier (BBB), is a significant obstacle to central nervous system (CNS) delivery of P-gp substrate drugs. Using positron emission tomography imaging, we investigated P-gp modulation at the human BBB by an approved P-gp inhibitor, quinidine, or the P-gp inducer, rifampin. Cerebral blood flow (CBF) and BBB P-gp activity were respectively measured by administration of ^{15}O-water followed by ^{11}C-verapamil. In a crossover design, healthy volunteers received quinidine and 11–29 days of rifampin treatment during different study periods. CBF and P-gp activity was measured in the absence (control; prior to quinidine treatment) and presence of P-gp modulation. At clinically relevant quinidine plasma concentrations, P-gp inhibition resulted in a 60% increase in ^{11}C-radioactivity distribution across the human BBB as measured by the brain extraction ratio (ER) of ^{11}C-radioactivity. Furthermore, the magnitude of BBB P-gp inhibition by quinidine was successfully predicted by a combination of in vitro and macaque data, but not by rat data. Although our findings demonstrated that quinidine did not completely inhibit P-gp at the human BBB, it has the potential to produce clinically significant CNS drug interactions with P-gp substrate drugs that exhibit a narrow therapeutic window and are significantly excluded from the brain by P-gp. Rifampin treatment induced systemic CYP3A metabolism of ^{11}C-verapamil; however, it reduced the ER by 6%. Therefore, we conclude that rifampin, at its usual clinical dose, cannot be used to induce P-gp at the human BBB to a clinically meaningful extent and is unlikely to cause inadvertent BBB-inductive drug interactions.

Introduction

Permeability-glycoprotein (P-gp), an ATP-binding cassette transporter and a member of the multidrug resistance (MDR) family, was one of the first xenobiotic transporters identified at the blood-brain barrier (BBB) (Schinkel et al., 1994; Borst and Schinkel, 2013). Due to its high expression at the BBB and wide substrate selectivity, P-gp is widely believed to be the most important transporter in modulating the entry of drugs into the central nervous system (CNS) (Sun et al., 2003).

We and others, using positron emission tomography (PET) imaging, have shown that inhibition of BBB P-gp by inhibitors [cyclosporine-A (CsA), tariquidar) can increase ^{11}C-verapamil (P-gp radiolabeled substrate) distribution into the human brain (Sasongko et al., 2005; Bauer et al., 2012). Because this increase in inhibition is modest, approved P-gp inhibitors that can inhibit human BBB P-gp to a greater extent are needed to further investigate the utility of P-gp inhibition to increase CNS drug delivery (e.g., treatment of brain tumors). Furthermore, using a combination of rat and MDR1-expressing cells, we successfully predicted the CsA–^{11}C-verapamil drug-drug interaction (DDI) at the human BBB (Hsiao et al., 2006). However, additional P-gp inhibitors need to be studied to further validate preclinical models for the prediction of P-gp–based DDIs at the human BBB. This is especially important for P-gp since it is known to exhibit multiple binding sites and demonstrates allosteric interactions (Martin et al., 2000; Zolnerciks et al., 2011).

Among the clinically approved drugs that can inhibit P-gp, quinidine, based on its ability to inhibit P-gp in vitro (EC_{50}: 0.9 μM) and its unbound therapeutic plasma concentration (C_u: 1.3 μM; C_u/EC_{50}: 1.4), is predicted to produce significantly greater inhibition (by ~4-fold) of P-gp at the human BBB than CsA (EC_{50}: 0.6 μM; C_u: 0.2 μM; C_u/EC_{50}: 0.3) (Hsiao et al., 2008; Brunton et al., 2011). Additionally, in humans, coadministration of quinidine with loperamide results in significant CNS toxicity of loperamide, a drug that is normally excluded from the CNS by BBB P-glycoprotein (Sadeque et al., 2000). Therefore, we hypothesized that if quinidine is found to be a more potent in vivo

This work was supported by the National Institutes of Health [Grants RCNS06804 and GM032165] and the National Center For Advancing Translational Sciences of the National Institutes of Health [Award Number UL1TR000423]. Li Liu was supported in part by the TL1 Multidisciplinary Predoctoral Clinical Research Training Program.

dx.doi.org/10.1124/dmd.114.058685.

ABBREVIATIONS: AhR, aryl hydrocarbon receptor; AIC, Akaike information criterion; AUC, area under the curve; AUCR, AUC_{blood}; BBB, Blood-brain barrier; C_u, unbound therapeutic plasma concentration; CAR, constitutive androstane receptor; CBF, cerebral blood flow; CI, confidence interval; CsA, cyclosporine-A; CV, coefficient of variation; DDI, drug-drug interaction; ER, extraction ratio; HPLC, high-performance liquid chromatography; MDR, multidrug resistance; MR, magnetic resonance; PET, positron emission tomography; P-gp, P-glycoprotein; PPB, plasma protein binding; PXR, pregnane X receptor; ROI, region of interest; 1-TC, one-tissue compartment.

inhibitor of P-gp at the human BBB than CsA, it could potentially be used clinically to overcome this P-gp barrier.

Conversely, studies using transgenic mouse models have shown that pretreatment of mice with rifampin induces BBB P-gp, resulting in a 70% decrease in methadone analgesia (Bauer et al., 2006). Similarly, pretreatment with pregnenolone 16α-carbonitrile (Ott et al., 2009) or dexamethasone (Chan et al., 2013) results in an increase of the efflux of known P-gp substrates, β-amyloid and quinidine, respectively. However, whether P-gp at the human BBB can be induced has never been investigated. Understanding the inducibility of BBB P-gp and determining the maximum magnitude of induction could help establish guidelines to prevent inadvertent DDIs with P-gp inducers that would decrease CNS drug delivery and, consequently, the efficacy of P-gp substrate drugs. Additionally, as demonstrated by the proof-of-concept studies in mice (Hartz et al., 2010), P-gp induction (e.g., by rifampin, dexamethasone) could be used to temporarily "tighten" the human BBB to prevent the entry of neurotoxins or xenobiotics (Bauer et al., 2006; Narang et al., 2008). If this can be demonstrated in humans, then inducing P-gp could be explored for the treatment of by restoring the P-gp activity found to be compromised in the Alzheimer's disease brain (Deo et al., 2014) and increasing the clearance of β-amyloid (Vogelgesang et al., 2002; Cirrito et al., 2005).

Therefore, in the study presented here, our objectives were to 1) quantify the ability of quinidine and rifampin to, respectively, inhibit and induce P-gp at the human BBB at therapeutic plasma concentrations of these drugs using ^{11}C-verapamil as the prototypic PET imaging agent, and 2) predict the resulting quinidine–^{11}C-verapamil DDI from preclinical experimental models.

Materials and Methods

Subjects. Ten healthy volunteers (six men and four women; 22–42 years of age; 61–98 kg) participated in the study. Potential subjects underwent a screening visit with medical history review, physical examination, EKG, complete blood cell count, hepatic and renal function tests, and pregnancy tests for women. Subjects were excluded if the aforementioned laboratory results were outside of the normal range or if the subjects had chronic medical conditions or were: breastfeeding, pregnant, smokers, taking long-term medications (except for stable doses of oral contraceptives for women), or had a history of substance abuse. No short-term medication (other than acetaminophen) was allowed for 24 hours before the PET imaging visit. Caffeine-containing beverages were not allowed on the day of study imaging. The study was approved by the University of Washington's Human Subjects Review Committee, Radiation Safety Committee, and Radioactive Drug Research Committee (Seattle, Washington). Informed consent was obtained from each subject.

Chemicals and Reagents. Racemic verapamil and verapamil metabolites (norverapamil, D-617, D-717) were obtained from the sources described previously (Sasongko et al., 2005). Solid-phase extraction C_8 cartridges (1 ml, 100 mg) were purchased from Varian (Lake Forest, CA). Ultrafiltration devices were purchased from Amicon Centrifree Micropartition Device (Bedford, MA). Quinidine gluconate and rifampin were provided by the University of Washington Medical Center Pharmacy (Seattle, WA). All other reagents were of the highest grade available from commercial sources.

Radiopharmaceuticals. The radiosynthesis of ^{15}O-water and ^{11}C-verapamil (from norverapamil) was as previously described (Sasongko et al., 2005). On the quinidine PET imaging day, when ^{15}O-water and ^{11}C-verapamil were administered twice in the same day, these PET tracers were freshly synthesized prior to their administration. All PET tracers were greater than 99% radiochemically and chemically pure, and had specific activity of approximately 53–61.3 TBq/mmol at the end of radiosynthesis and 33.6–41 TBq/mmol at the time of all injections. On average, 10.82 mCi or 4.65 μg of ^{11}C-verapamil was administered at each imaging session. ^{3}H-verapamil (verapamil [*N*-methyl ^{3}H] hydrochloride; 2.2 TBq/mmol) for verapamil plasma protein binding assays was purchased from American Radiolabeled Chemicals, Inc. (St. Louis, MO).

Experimental Study Design. The study was divided into two arms in a crossover design with quinidine and 11–29 days of rifampin treatment administered during different study periods (Fig. 1A). Subjects in arm A (n = 7) were first imaged in the absence (control scan) or presence of quinidine (consecutive studies on the same day). They were then imaged again after at least 11–29 days of rifampin treatment (600 mg once daily at night). Subjects in arm B (n = 3) were studied in the reverse order, e.g., first imaged after at least 11–29 days of rifampin treatment followed by 21–42 days of washout, and then imaged in the absence (control) or presence of quinidine.

A power analysis was conducted to determine the study sample size using data from a previous CsA-verapamil PET imaging study in healthy volunteers (Sasongko et al., 2005). In this study, the coefficient of variation (CV) of AUC_{blood} (AUCR) [^{11}C-radioactivity area under the curve (AUC) in the brain/^{11}C-radioactivity AUC in the blood in the presence and absence of CsA] was 22%. Since a difference in ^{11}C-verapamil brain distribution of $<$30% in the presence of an inhibitor is unlikely to be clinically significant (intrasubject variability in pharmacokinetics of most drugs tends to be at least that), we used this as a cutoff for a significant DDI at the human BBB. Under these assumptions, our analysis indicated that nine subjects per treatment (quinidine or rifampin) were sufficient to provide 80% power with $\alpha = 0.05$ to detect at least a 30% change in brain distribution of ^{11}C-verapamil.

On the imaging days, a pregnancy test was performed on female volunteers, which was required to be negative. Each subject had catheters inserted in both arms (antecubital veins), one with two separate lines for PET tracer injections and quinidine venous blood sampling, and the other catheter for quinidine infusion. In the arm used for quinidine infusion, the radial artery was catheterized for arterial blood sampling during PET imaging. Quinidine gluconate (80 mg/ml; Eli Lilly, Indianapolis, IN) was formulated for intravenous infusion as per instructions in the manufacturer's package insert, and administered at rates detailed in Fig. 1B. Each subject's head was immobilized during the PET imaging studies using a custom-made thermoplastic mask and head-holder.

The PET imaging experimental design and image acquisition (GE Advance PET camera, Little Chalfont, UK) of the control and quinidine treatment followed the study sequence described previously with the modifications illustrated in Fig. 1B (Sasongko et al., 2005). The experimental design and timeline for the postrifampin PET imaging were identical to that in the control arm. In brief, during all three PET imaging sessions (control, quinidine, postrifampin treatment), subjects were administered ^{15}O-water (~0.5 mCi/kg, i.v. bolus) and ^{11}C-verapamil (~0.1 mCi/kg, $<$0.08 μg/kg, 1-minute i.v. infusion) consecutively, separated by ~15 minutes, and brain PET images were acquired to determine cerebral blood flow (CBF) and P-gp activity, respectively. Within 1 week of the PET studies, the subjects underwent magnetic resonance (MR) imaging of the brain [T1- and T2-weighted images; Philips Achieva 3 Tesla Scanner (Andover, MA)] to provide anatomic information for the construction of region-of-interest (ROI) PET analysis. Subjects were evaluated poststudy (1–2 weeks after the imaging session), with all tests performed at the screening visit, except for the EKG and the pregnancy test.

Blood Sample Collection and Processing. Arterial blood samples (1 ml) during both PET imaging sessions (control and quinidine treatment) were manually collected as follows: ^{15}O-water (first 1 minute: every 5 seconds; 1–2 minutes: every 15 seconds; 2–4 minutes: every 30 seconds; and then at 5 minutes) and ^{11}C-verapamil (first 1 minute: every 15 seconds; 1–2 minutes: every 20 seconds; 2–3 minute: every 30 seconds; 3–8 minutes: every 1 minute; 8–12 minutes: every 2 minutes; and then at 15 and 20 minutes). ^{15}O-water blood radioactivity in preweighed gamma-counting tubes and ^{11}C-verapamil blood and plasma radioactivity were determined using a gamma counter (Cobra Counter; Packard Corporation, Meriden, CT).

In addition, arterial blood samples (2 ml) were manually collected during all three ^{11}C-verapamil PET imaging sessions at 5, 10, and 20 minutes to quantify the radioactivity content of ^{11}C-verapamil, its known ^{11}C-dealkylated metabolites (D-617, D-717), and ^{11}C-N-demethylated metabolites (polar species) in the plasma at control, in the presence of quinidine and postrifampin treatment via solid-phase extraction and high-performance liquid chromatography (HPLC) methods described previously (Sasongko et al., 2005, Unadkat et al., 2008).

Quantification of Quinidine Plasma Concentration. To measure quinidine plasma concentrations, venous blood samples (2 ml) were drawn at 0, 15, 30, 45, 60, and 80 minutes after the start of quinidine infusion (or the last sample was taken at the end of the second ^{11}C-verapamil PET imaging). The calibrators were

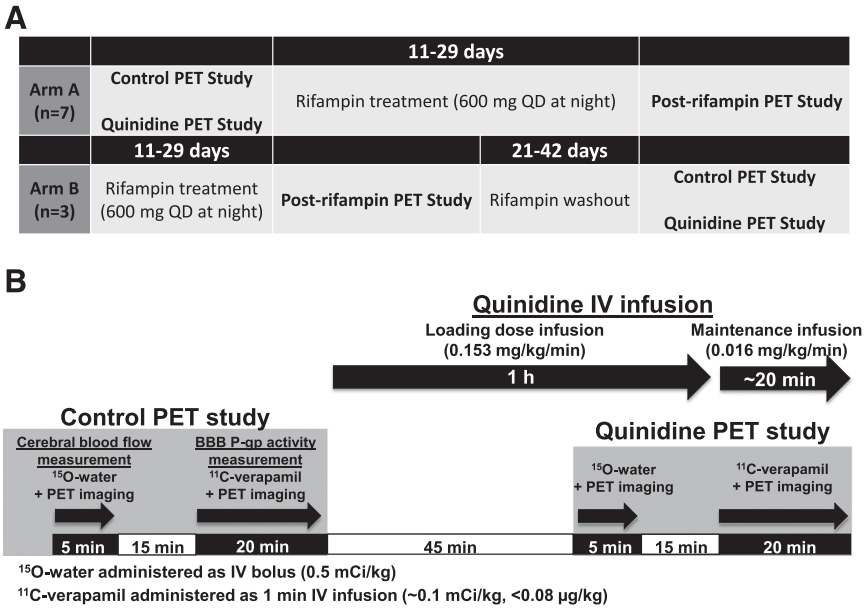

Fig. 1. (A) PET study design. (B) Timeline for administration of the PET tracers, ^{15}O-water and ^{11}C-verapamil, to assess, respectively, CBF and BBB P-gp activity in the absence or presence of quinidine treatment. Quinidine PET scans were performed on the same day as the control. Design and timeline for the postrifampin PET scans were identical to those used in the control arm. QD, once daily.

prepared in human plasma (quinidine concentration range: 1–15 μM). Quality control samples (quinidine concentrations: 1, 4, and 15 μM) were prepared and processed along with the venous plasma samples collected during the PET imaging studies. All plasma samples (800 μl) were spiked with an equal volume of acetonitrile containing 1 μg/ml Hoechst 33258 (internal standard) and processed in duplicate as previously described (Reece and Peikert, 1980). The supernatants were then reconstituted in the HPLC mobile phase (initial elution gradient condition), and 50 μl was injected onto the HPLC. HPLC separation was achieved using an Agilent (Santa Clara, CA) XDB C18 2.1 $\times$ 50 mm, 5 μm column, and the analytes (quinidine at 250 nm, retention time 3.5 minutes; internal standard: Hoechst 33258 at 350 nm, retention time 5 minutes) were eluted with 1% formic acid and 0.1 M potassium phosphate in water at pH 3.30 (solvent A) and 1% formic acid in acetonitrile (solvent B). For the first 3 minutes, the gradient was maintained at 90% solvent A, decreased linearly to 60% solvent A until 8 minutes, and then cycled back to initial conditions.

Verapamil Plasma Protein Binding. To ensure that chronic administration of rifampin and the presence of quinidine did not significantly increase verapamil plasma protein binding, ultrafiltration was used to quantify and compare verapamil plasma protein binding in pooled plasma samples (n = 3 subjects) collected during control, quinidine, and postrifampin treatment PET imaging sessions. Pooled plasma samples were used due to the limited plasma volume available. Six hundred microliters of the plasma was spiked with ^{3}H-verapamil (20 nCi/ml) and incubated at 37°C for 20 minutes, in triplicate. At the end of the incubation, 500 μl of the plasma was transferred into the ultrafiltration device and centrifuged (2000g) at 37°C for 10 minutes. Radioactivity in 100 μl of the plasma or ultrafiltrate was then determined by radioactivity scintillation counting. Verapamil plasma protein binding was calculated by the difference in plasma and the ultrafiltrate radioactivity expressed as a percentage of plasma radioactivity (Sasongko et al., 2005).

Image Processing. Both the PET image acquisition and reconstruction were conducted as described previously (Sasongko et al., 2005). MR images were coregistered to the PET images with a method based on mutual information criteria using PMOD software (PMOD Technologies, Zurich, Switzerland). ROIs for three tissue types/brain regions (whole brain, gray matter, or white matter for both hemispheres) were identified manually on the coregistered PET-MR images to avoid margins of the respective tissues, and extended continuously to an average of 18 slices (~6 cm) to create volumes of interest for each tissue type. Volumes of interest were applied to both the ^{15}O-water and ^{11}C-verapamil dynamic images to determine decay-corrected radioactivity concentration in each brain region.

Noncompartmental Analysis. After decay correction, the area under the ^{11}C-verapamil radioactivity concentration-time curve in the brain region ($AUC_{brain\ region}$; whole brain, gray matter, or white matter) and blood (AUC_{blood}) was calculated from ^{11}C-verapamil PET imaging in the control arm, in the presence of quinidine, or postrifampin treatment using the trapezoidal rule. The percent change in the ratio of $AUC_{brain\ region}$: AUC_{blood} (AUCR) was used to evaluate the magnitude of BBB P-gp modulation by quinidine or rifampin treatment.

Compartmental Analysis. Regional CBF for the whole brain, gray matter, or white matter was estimated for each subject by fitting a flow-dispersion model to the first 2 minutes of the ^{15}O-water tissue time-activity curves in the respective brain tissue using the PKIN module in PMOD.

Previously, a one-tissue compartment (1-TC) compartment model was shown to be the best model to estimate the distribution clearance of ^{11}C-verapamil into the human brain (K1) (Muzi et al., 2009). In fact, we and others have confirmed that, when P-gp activity at the human BBB is inhibited, it is the K1 of ^{11}C-verapamil radioactivity into the brain that is changed, rather than the efflux rate constant out of the brain (k2) (Bauer et al., 2006; Bankstahl et al., 2008, Liow et al., 2009; Kreisl et al., 2010). To confirm this finding, we analyzed our data using a 1-TC model with different a duration of data sets (5, 10, or 20 minutes) and input functions [total plasma radioactivity, ^{11}C-verapamil and ^{11}C-verapamil metabolites that are P-gp substrates (^{11}C-dealkylated metabolites), or a dual input function that simultaneously and separately modeled the ^{11}C-radioactivity contributed by P-gp substrates and non–P-gp substrates (^{11}C-polar metabolites)] using PKIN software (PMOD Technologies). An average value of human brain tissue blood volume (V_b: 0.044 ml/g) determined previously (Muzi et al., 2009) was incorporated as a fixed constant when estimating CBF and $K1_p$ (based on plasma data) and k2. Weights were set at 1/(observed radioactivity)^2. The best model was determined by evaluating the Akaike information criterion (AIC), runs test, visual inspection of the residuals and model fits, and percent CV of the final estimates. To determine the brain extraction ratio (ER) of ^{11}C-verapamil radioactivity (based on blood data), the ratio of $K1_b$ ($K1_p$ corrected for the individual blood-to-plasma ratio) and CBF was computed. The correlation (correlation coefficient) between $K1_b$ and AUCR values was determined using Microsoft Excel (Microsoft Software, Redmond, WA).

Statistical Analysis. Data are expressed as the mean $\pm$ S.D. As pharmacokinetic data are typically log-normally distributed, the AUCR, $K1_b$, and ER data were logarithmically transformed and analyzed using a Student's paired one-tail t test. The latter approach is justified as our a priori hypothesis was that quinidine or rifampin treatment would produce unidirectional changes, inhibition, or induction, respectively, to P-gp activity at the BBB. The primary endpoint of the study is the ER. The ratio of each endpoint in the presence and absence of the modulator (quinidine or rifampin) and the corresponding 95% confidence intervals (CIs) were determined and transformed back to the original scale for presentation. All comparisons and corresponding confidence intervals were adjusted for the two comparisons (rifampin, verapamil) using the Bonferroni method. Significance level was set at $P < 0.05$.

Results

Ten volunteers participated in the study without any unexpected side effects. Of these 10 volunteers, for reasons unrelated to the treatments of the study, one did not have the quinidine verapamil PET images due to computer mechanical errors (missing verapamil attenuation scans), and one voluntarily withdrew from the study after the control and quinidine scans and did not complete the postrifampin scan. Therefore, nine sets of complete data sets were available for each treatment (quinidine or postrifampin).

Verapamil percentage unbound in the plasma was consistent with the literature-reported value of 10% (Brunton et al., 2011) and did not differ significantly between control versus quinidine (7.6 ± 0.7% vs. 9.1 ± 0.9%; $P > 0.05$) or between control versus rifampin (8 ± 0.7% vs. 7 ± 0.9%; $P > 0.05$). The blood-to-plasma ratio of ^{11}C-verapamil during PET imaging was not significantly affected by quinidine (control 0.77 ± 0.06 vs. quinidine 0.81 ± 0.08; $P > 0.05$) or rifampin (control 0.76 ± 0.05 vs. rifampin 0.77 ± 0.08; $P > 0.05$). Similarly, quinidine or rifampin treatment did not significantly affect CBF, or the regional CBF difference between white matter and gray matter (Fig. 2). The absolute CBF values estimated in the control arm for the gray matter and white matter were consistent with historical data compiled from multiple published studies (Reich and Rusinek, 1989). However, the individual CBF did vary significantly; therefore, the individual CBF values were used for all subsequent data analysis.

The accuracy and precision of the quinidine assay based on the three quality control samples were acceptable (<12% error and <5% CV). The average total pseudo steady-state quinidine plasma concentration achieved during the second ^{11}C-verapamil PET imaging session was 8.3 ± 1.4 μM (1.3 ± 0.3 μM unbound determined based on literature-reported quinidine plasma protein binding; Brunton et al., 2011) and was within the therapeutic range (8–15 μM).

As expected, quinidine (a potent CYP2D6 inhibitor) treatment had no significant ($P > 0.05$) effect on ^{11}C-verapamil metabolism (Fig. 3), which is primarily mediated by CYP2Cs and CYP3A4 to form the ^{11}C-dealkylated metabolites (P-gp substrates) and ^{11}C-N-demethylated metabolites (polar species and non–P-gp substrates), respectively (Tracy et al., 1999; Pauli-Magnus et al., 2000). Similar to our previous findings, at 5 and 10 minutes of the PET imaging sessions, ~85% of the total plasma radioactivity was attributed to P-gp substrates, with little contribution from non–P-gp substrates. Therefore, for the determination of quinidine's impact on P-gp activity, all subsequent data analyses (including estimation of AUCR) were performed using data collected during the first 10 minutes of PET imaging.

On the other hand, rifampin, a selective pregnane X receptor (PXR) ligand and a potent inducer of PXR-regulated cytochrome P450 genes (e.g., CYP3A), did induce hepatic ^{11}C-verapamil metabolism. This manifested as a significant increase (~2-fold compared with control; $P < 0.05$) in the 10-minute plasma content of CYP3A-formed ^{11}C-polar metabolites (non–P-gp substrates) of ^{11}C-verapamil (Fig. 4). However, after rifampin treatment, no significant change was observed in the plasma content of the ^{11}C-dealkylated metabolites (P-gp substrates) of ^{11}C-verapamil formed by CYP2Cs. In contrast, over the shorter time frame of 5 minutes, the ^{11}C-radioactivity composition in plasma in the control arm or postrifampin treatment was not significantly different ($P > 0.05$). Based on this minimal metabolism of ^{11}C-verapamil and significant ^{11}C-radioactivity distribution into the brain during the first 5 minutes of ^{11}C-verapamil PET imaging, this shorter time frame was chosen as the time interval for all subsequent data analyses (including estimation of AUCR). Furthermore, as indicated later, analysis over a longer time frame (10 or 20 minutes) did not change our conclusion.

Quinidine significantly increased the brain tissue radioactivity concentration, as illustrated in Fig. 5. The distributions of ^{11}C-verapamil radioactivity (as measured by the AUCR over 10 minutes) into the brain, expressed as a ratio of AUCR in the presence and absence of quinidine (95% CI), were as follows: whole brain, 1.58 (1.28–1.96); gray matter, 1.57 (1.27–1.95); or white matter, 1.63 (1.30–2.03) (Fig. 6A, shown with absolute untransformed values and P values). The AUCR was significantly greater for the gray matter than for the white matter in the control arm versus in the presence of quinidine.

Consistent with our previous finding (Muzi et al., 2009), a 1-TC model using the single input function consisting of total plasma radioactivity (10-minute data: AIC value of 19 vs. 20-minute data: AIC value of 20) for estimating $K1_p$ and k_2 of ^{11}C-verapamil radioactivity in the control arm versus in the presence of quinidine was equivalent to or better than using other input functions [^{11}C-verapamil radioactivity contributed by P-gp substrates (10-minute data: AIC value of 24 vs. 20-minute data: AIC value of 23) or dual input function of ^{11}C-verapamil radioactivity contributed by P-gp substrates or non–P-gp substrates (10-minute data: AIC value of 21 vs. 20-minute data: AIC value of 19)]. To minimize the potential for ^{11}C-verapamil metabolites confounding our results, we limited our data analysis to the first 10 minutes. Quinidine significantly increased $K1_b$ of ^{11}C-verapamil radioactivity into the brain, expressed as a ratio of $K1_b$ in the

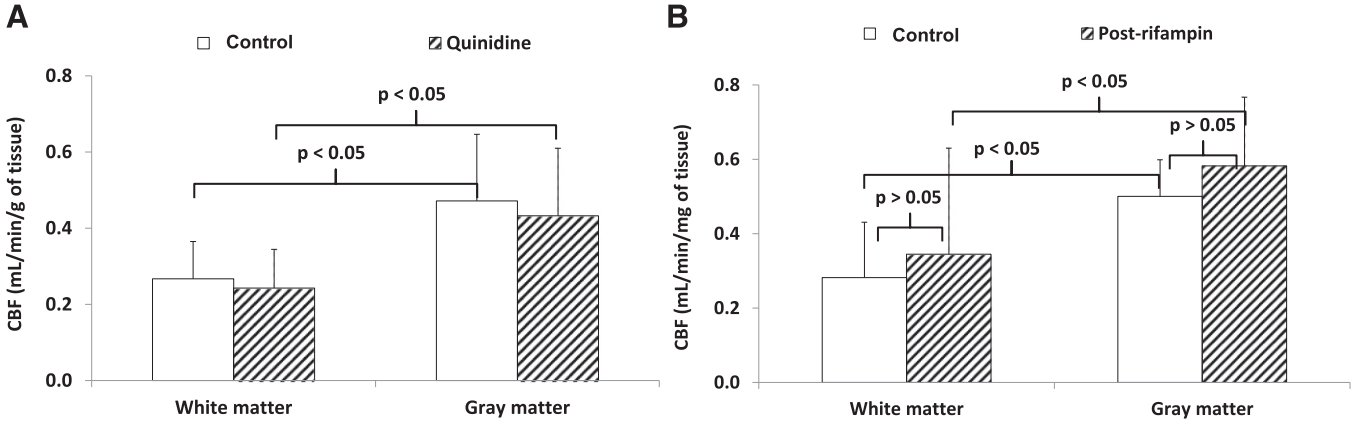

Fig. 2. CBF was estimated by fitting a flow-dispersion model to 2 minutes of the ^{15}O-water plasma and tissue time-activity curves. Significant interindividual variability in CBF was observed across different subjects, and therefore, individual CBF values were used for all subsequent data analyses. CBF was unaffected by the presence of quinidine (A) or postrifampin treatment (B). Data are expressed as the mean ± S.D. (n = 9).

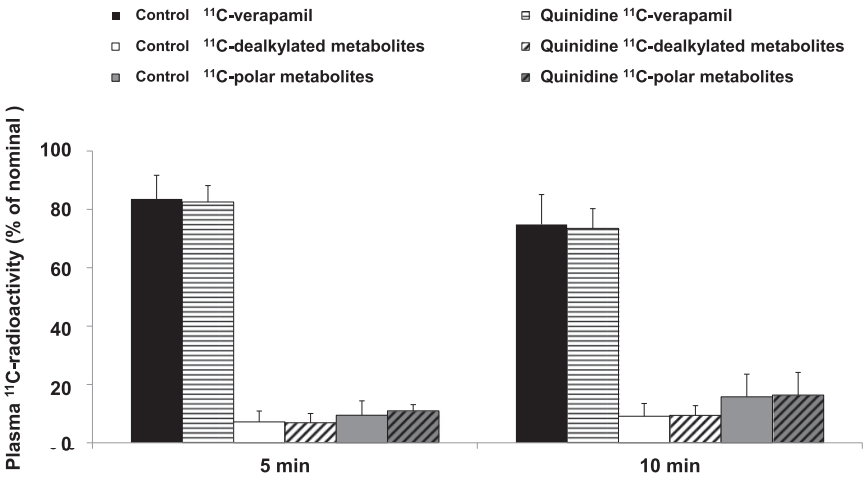

Fig. 3. The plasma content of ^{11}C-verapamil and its circulating ^{11}C-dealkylated metabolites and ^{11}C-N-demethylated (polar species) metabolites at 5 or 10 minutes of the PET imaging sessions was unaffected by the presence of quinidine. Percentage of nominal refers to radioactivity in the solid-phase extraction extracts relative to the total radioactivity in the plasma sample prior to solid-phase extraction analysis. Nearly 100% of the ^{11}C-radioactivity in all samples was recovered after the solid-phase extraction analysis and confirmed by HPLC. At both time points, ~85% of the total plasma radioactivity was attributed to P-gp substrates (^{11}C-verapamil, ~75%; its ^{11}C-dealkylated metabolites, ~10%), with little contribution from non–P-gp substrates (^{11}C-N-demethylated metabolites or polar metabolites, ~15%). Data are expressed as the mean ± S.D. (n = 9).

presence and absence of quinidine (95% CI), as follows: whole brain, 1.37 (1.21–1.55); gray matter, 1.35 (1.20–1.51); and white matter, 1.48 (1.27–1.73) (Fig. 6B). However, quinidine treatment did not affect k_2 (e.g., gray matter, control: 0.1 ± 0.01 minute^{-1}; quinidine: 0.1 ± 0.02 minute^{-1}). Additionally, quinidine significantly increased the ER of ^{11}C-verapamil radioactivity by the brain, expressed as a ratio of ER in the presence and absence of quinidine (95% CI), as follows: whole brain, 1.56 (1.01–2.42); gray matter, 1.53 (0.98–2.37); or white matter, 1.71 (1.10–2.68) (Fig. 6C). After CBF normalization (reported as ER), the large regional difference observed in the $K1_b$ of ^{11}C-verapamil radioactivity between gray matter and white matter in the control arm and in the presence of quinidine was greatly diminished (Fig. 6C), again emphasizing the utility of ER to measure P-gp activity at the human BBB. Additionally, the larger variability associated with CBF increased the intersubject variability in P-gp inhibition after CBF normalization. This variability could not be attributed to differences in plasma concentration of quinidine. Last, the $K1_b$ and AUCR of ^{11}C-verapamil radioactivity were significantly correlated for the whole brain, gray matter, and white matter, with correlation coefficients of 0.82, 0.84, and 0.85, respectively, which emphasizes that the uptake of ^{11}C-radioacitivity across the human BBB increased consistently using either endpoint.

After rifampin treatment, the ratio of AUCR in the presence and absence of rifampin treatment (95% CI) was as follows: whole brain, 1.09 (0.81–1.46); gray matter, 1.08 (0.80–1.45); or white matter, 1.09 (0.79–1.49) (Fig. 7A). Similar to the regional CBF differences, the distribution of ^{11}C-verapamil radioactivity (as measured by AUCR) into gray matter was significantly greater than that into white matter in the control arm or after rifampin treatment.

After evaluating the goodness of fit of the 1-TC model, using different plasma radioactivity input functions and data of different imaging durations (5, 10, or 20 minutes), the best model for the data was when the total plasma ^{11}C-radioactivity was used as the input function (AIC values for control and postrifampin treatment of 19 and 13, respectively, vs. AIC values of 23 and 17 using other input functions). This is consistent with our previous findings from the CsA–^{11}C-verapamil PET study (Sasongko et al., 2005). Using this input function, we found that the $K1_p$ estimates were similar, irrespective of the duration of data used (5, 10, or 20 minutes). However, since the ^{11}C-verapamil plasma metabolite content at 5 minutes was the least and not significantly affected by rifampin treatment, to minimize the contribution of these metabolites from confounding our data interpretation, we limited all our modeling analysis to the first 5 minutes of the ^{11}C-verapamil PET imaging. However, as indicated later, analysis over a longer time frame (10 or 20 minutes) did not change our conclusions. Our results showed that, after chronic rifampin treatment, the ratio of $K1_b$ in the presence and absence of rifampin treatment (95% CI) was as follows: whole brain, 1.01 (0.78–1.31); gray matter, 1.00 (0.79–1.28); or white matter, 0.98 (0.69–1.40) (Fig. 7B). Likewise, after rifampin treatment, the ratio of ER in the presence and absence of rifampin

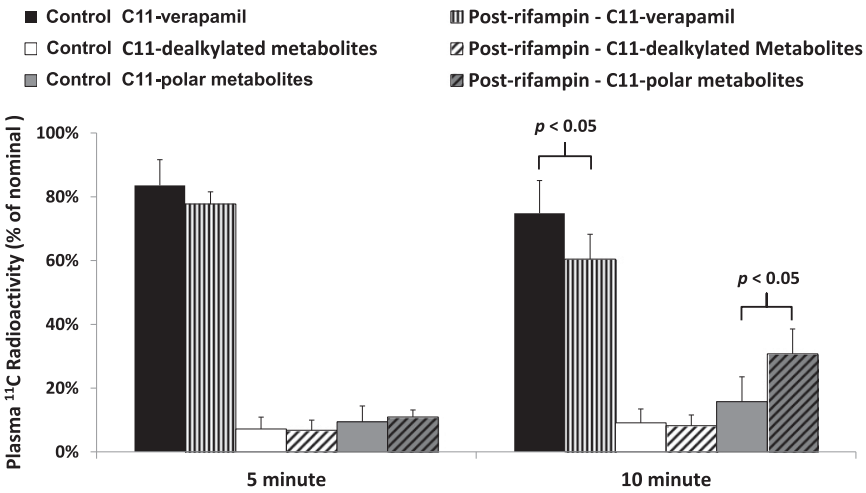

Fig. 4. Plasma ^{11}C-verapamil polar metabolite (formed by CYP3A) contents at 5 minutes after ^{11}C-verapamil administration during baseline and postrifampin PET imaging sessions were not significantly different, whereas those at 10 minutes were. In contrast, the plasma contents of ^{11}C-dealkylated metabolites (formed by CYP2Cs) during baseline and postrifampin PET imaging session were not significantly different at 5 or 10 minutes. Data are expressed as the mean ± S.D. (n = 9).

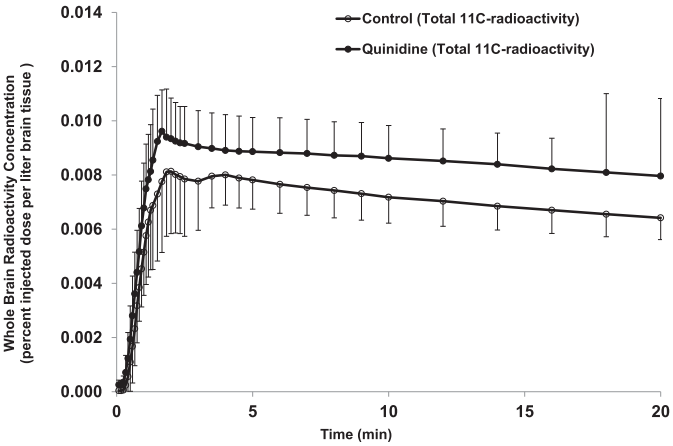

Fig. 5. Dose-normalized mean whole-brain radioactivity concentration versus time profiles (total ^{11}C-radioactivity) in the absence (control) and presence of quinidine. Data are expressed as the mean ± S.D. (n = 9).

treatment (95% CI) was as follows: whole brain, 0.94 (0.59–1.50); gray matter, 0.94 (0.60–1.48); or white matter, 0.88 (0.52–1.48) (Fig. 7C). Additionally, k_2 was also unaffected (e.g., gray matter: control 0.14 ± 0.04 minute^{-1} vs. postrifampin 0.15 ± 0.03 minute^{-1}). After normalizing $K1_b$ to CBF, the regional difference (gray matter vs. white matter) observed for $K1_b$ was greatly diminished, as shown by similar ER values in the control arm (gray matter: 0.16 ± 0.05, white matter: 0.13 ± 0.05) or postrifampin treatment (gray matter: 0.16 ± 0.08, white matter: 0.12 ± 0.06).

To investigate whether the quinidine–^{11}C-verapamil DDI at the human BBB could be equally well predicted from preclinical studies as the CsA–^{11}C-verapamil DDI, we evaluated the ability of two animal models, the rat and the macaque, in combination with in vitro data in MDR1-expressing cells to predict the magnitude of P-gp inhibition by quinidine at the human BBB. Based on the maximal increase in the distribution of ^{11}C-verapamil radioactivity into the animal brains (Hsiao et al., 2006; Eyal et al., 2009) when P-gp was completely inhibited (macaque: 3.4-fold, rat: 9.2-fold), the fraction transported (f_t) by P-gp was computed (macaque: 0.73; rat: 0.91). We then assumed that the inhibitory properties of quinidine (in vitro EC_{50}: 0.9 μM and γ: 0.8) determined using LLCPK cells stably transfected with MDR1 (Hsiao et al., 2008) apply to the in vivo inhibition of P-gp at the human BBB. Based on these data and assumptions, our observed quinidine–^{11}C-verapamil DDI (~70% increase in ER) at the human BBB was better predicted from the in vivo macaque data (~112%) than the in vivo rat data (554%) at the average plasma quinidine unbound concentration (C_u = 1.3 μM) observed in our study.

Discussion

Our study design, investigation, and data analysis took into consideration factors that could potentially impact our data interpretation, such as changes in CBF, ^{11}C-verapamil plasma protein binding (PPB), or ^{11}C-verapamil metabolism. We measured CBF because we have previously shown that, to unambiguously measure changes in P-gp activity at the human BBB, without the confounding factor of changes in CBF, one must take into consideration CBF (Eyal et al., 2010). Both quinidine and rifampin did not impact CBF or PPB of ^{11}C-verapamil. For the latter, although this conclusion cannot be made definitive due to the fact that the sample was pooled, the small increase in the actual observed value of PPB in the presence of quinidine cannot completely explain the observed increase in ER. This ensures that our interpretation of P-gp modulation by the two drugs was not confounded by potential transient increase in the unbound ^{11}C-verapamil plasma concentration that could result from PPB displacement interaction. Similarly, we avoided confounding of our interpretation of our data due to metabolism of ^{11}C-verapamil by confining our data analysis to a duration where it was minimal (5 and 10 minutes for rifampin and quinidine treatment, respectively).

To evaluate P-gp modulation by quinidine or rifampin, we used two approaches in analyzing our data, compartmental and noncompartmental analyses. The compartmental approach allows one to discern the influence of CBF or ^{11}C-verapamil metabolites on the brain distribution of ^{11}C- radioactivity, and dissect mechanistically which parameter, $K1_b$ or k_2, is affected when P-gp is modulated. Then, $K1_b$ is used to derive ER ($K1_b$ /CBF), which is a measure of P-gp activity at the BBB unencumbered by any changes in CBF (Eyal et al., 2010). The endpoint, ER, accounts for intertreatment variability in CBF when P-gp modulation is measured using a highly permeable and lipophilic PET ligand such as verapamil. Therefore, consistent with Liow et al. (2009) and our previous paper (Eyal et al., 2010), we used ER, rather than $K1_b$ and AUCR, as a primary measure of P-gp activity and its modulation at the BBB.

Analysis of our data by compartmental modeling showed that the 1-TC compartment model using the single input function of total plasma radioactivity provides the best fit to the first 5 and 10 minutes of ^{11}C-verapamil PET imaging data from the rifampin and quinidine studies, respectively. As we hypothesized, these data suggest that the ^{11}C-dealkylated metabolites behaved like ^{11}C-verapamil with respect to their distribution into the brain, and the ^{11}C-polar metabolites exerted minimal impact on the estimation of $K1_p$. Mechanistically, P-gp substrates can be efficiently extracted by P-gp from the membrane bilayer while in transit through the membrane, and/or effluxed out by P-gp after entering the intracellular compartment (Aller et al., 2009). Both mechanisms should result in increased ER (and $K1_b$) of P-gp substrates into the brain when P-gp, the gatekeeper at the BBB, is modulated. Indeed, quinidine inhibition of P-gp significantly increased $K1_b$ into the brain (e.g., 35% for gray matter) with no significant change in k_2 (e.g., 3% for gray matter). This is consistent with previous results using the same or different P-gp PET ligands (Bankstahl et al., 2008; Liow et al., 2009; Kreisl et al., 2010; Bauer et al., 2012).

The noncompartmental or the AUCR approach, however, is useful in that it is nonparametric and therefore free of any compartmental model assumptions. In the present study, the AUCR is reflective of the distribution clearance or initial uptake of ^{11}C-radioactivity into the brain, as it is unlikely that ^{11}C-radioactivity achieved brain:plasma pseudo equilibrium within the 5- to 10-minute time frame. At the average plasma quinidine unbound concentration achieved during the second ^{11}C-verapamil PET imaging session, AUCR increased by ~60% for all brain regions studied. Altogether, AUCR reflected the increased $K1_b$ of ^{11}C-verapamil radioactivity into the brain as shown by the excellent correlation between the two parameters.

In an abstract, Passchier et al. (2008) reported a lack of DDI between quinidine and ^{11}C-loperamide at the human BBB. However, in that study, the dosing regimen and route of quinidine administration were not provided, nor were the quinidine plasma concentrations measured. If a single dose of oral quinidine were administered (approximately 600-mg quinidine base), the quinidine peak plasma concentration achieved, which is transient following a single dose, is approximately 2.5 mg/l (7.4 μM; Frigo et al., 1977). The calculated average plasma concentration over the dose interval is approximately 1.2 mg/l (3.7 μM; Frigo et al., 1977). Based on our data, these concentrations are unlikely to significantly inhibit P-gp at the human BBB.

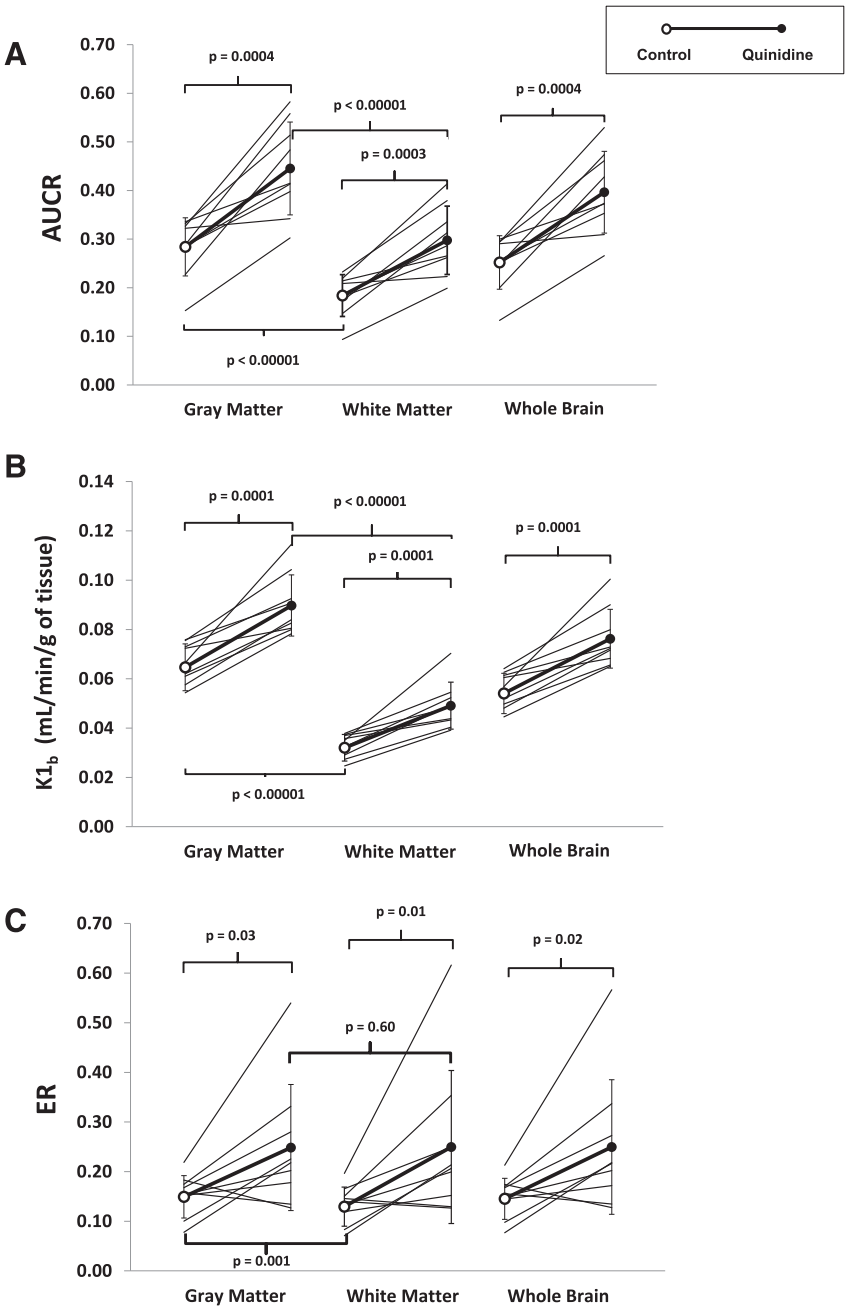

Fig. 6. Quinidine significantly ($P < 0.05$) increased the mean distribution of ^{11}C-verapamil radioactivity into the whole brain, gray matter, or white matter as measured by the AUCR (A), distribution clearance ($K1_b$) (B), or ER (C). Of note, the AUCR and $K1_b$ of ^{11}C-verapamil radioactivity were significantly greater for the gray matter than the white matter (at control and in the presence of quinidine). These regional differences were considerably reduced when the ER for these regions was computed. Both individual (n = 9) and mean (expressed as the mean ± S.D.) are shown.

The observed modest magnitude of P-gp inhibition by quinidine (ER in the presence of quinidine is much smaller than 1) was likely due to incomplete inhibition of P-gp. This can be determined via further evaluation of ER (but not $K1_b$, again highlighting the advantage of the use of ER). The ER value enables estimation of the maximum possible magnitude of increase in the CNS delivery of drugs when P-gp is completely inhibited (i.e., maximum liability of DDI) and when only the control ER is available through PET studies (the usual case). For a lipophilic and highly permeable drug, when P-gp is completely inhibited, the extraction of the drug by the brain may be so efficient as to be limited by CBF, and the ER = 1. Indeed, we confirmed this by demonstrating that the ER of ^{11}C-verapamil radioactivity in the pituitary gland (outside the BBB and lacks P-gp; Nussey and Whitehead, 2001) was close to unity (1.13 ± 0.02; Eyal et al., 2010). Using a similar approach and our current data, we estimated this maximum change in the ER to be ~6-fold. This estimate is reasonable, as the macaque or human ^{11}C-verapamil brain uptake increased by ~3- to 4-fold in the presence of CsA or tariquidar, respectively (Bauer et al., 2012; Eyal et al., 2009). It is important to note that the magnitude of change in drug distribution into the brain due to P-gp inhibition is substrate-dependent, and may be considerably greater for substrates (e.g., *N*-desmethyl-loperamide or nelfinavir) (Kaddoumi et al., 2007; Seneca et al., 2009), where P-gp plays an even greater role in excluding them from the brain, i.e., when the fraction transported (f_t) by P-gp is even larger than that for verapamil (Hsiao and Unadkat, 2014). Consequently we conclude that, similar to CsA, quinidine is not a suitable drug to markedly inhibit P-gp at the human BBB to increase CNS delivery of drugs.

The macaque and not the rat, in combination with in vitro data in MDR1-expressing cells, was better able to predict the magnitude of

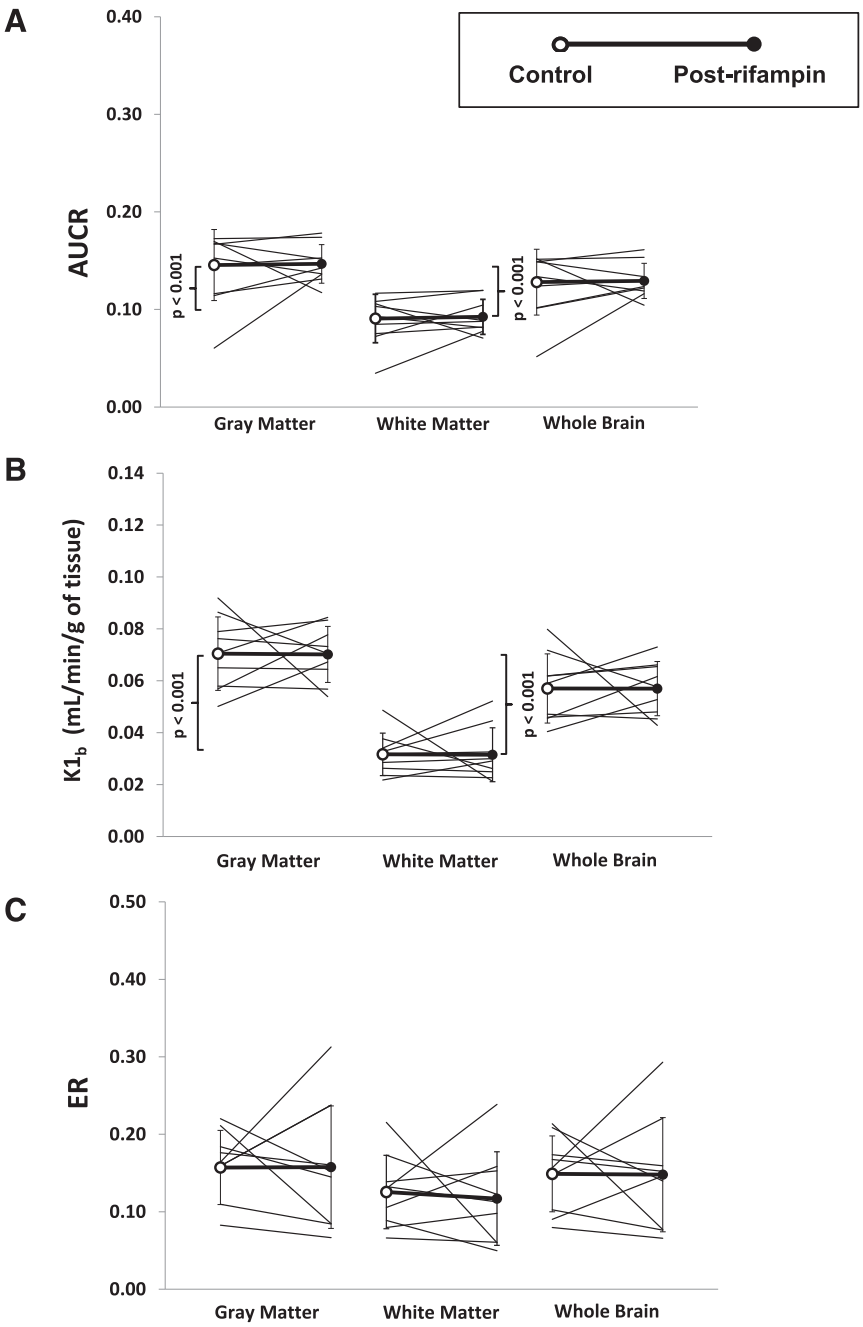

Fig. 7. After rifampin treatment (600 mg once daily at night), no significant change was observed in the AUCR (A), $K1_b$ (B), or ER (C), indicating that P-gp activity at the human BBB was not induced. Of note, the AUCR and $K1_b$ of ^{11}C-verapamil radioactivity were significantly greater for the gray matter than the white matter (in the control and postrifampin arm). These regional differences were eliminated when the ER for these regions was computed. Both individual (n = 9) and mean (expressed as the mean ± S.D.) are shown.

P-gp inhibition by quinidine at the human BBB. This discrepancy between the two predictions could be due to either the MDR1 cells not accurately reporting the in vivo inhibitory characteristics (EC_{50} and γ) of quinidine or the dynamic range of P-gp inhibition in the rat overpredicting the corresponding dynamic range in humans. The latter is possible as CBF in the rat is approximately twice that in humans (Yuen et al., 2008), and P-gp protein expression at the macaque and human BBB is similar, but ~2-fold lower than that at the rat BBB (Ito et al., 2011; Shawahna et al., 2011; Uchida et al., 2011). These explanations are not completely satisfactory, as the CsA–^{11}C-verapamil DDI at the human BBB was well predicted by the rat data (Hsiao et al., 2006). On the other hand, this discordance is unsurprising since P-gp exhibits allosterism with multiple ligand binding sites, such that the magnitude of P-gp–based DDI may be dependent on both the inhibitor and substrate.

To date, in vivo induction of P-gp at the human BBB has never been studied. Here, we investigated for the first time whether rifampin, at doses that induce intestinal P-gp activity, can induce P-gp activity at the human BBB. We chose rifampin as our prototypic P-gp–inducing agent because it is the most potent Food and Drug Administration–approved P-gp inducer. Numerous healthy volunteer studies have shown that oral administration of rifampin (600 mg once daily for as few as 6 days) induces intestinal P-gp as measured by the increased oral clearance and decreased plasma AUC of digoxin, fexofenadine, or talinolol (Hamman et al., 2001; Niemi et al., 2003; Gurley et al., 2008). The same rifampin dosing regimen induces intestinal CYP3A and P-gp expression to a similar extent. Therefore, we followed this standard P-gp induction protocol and instructed all human volunteers to take rifampin orally once a day (600 mg) for 11–29 days to determine if P-gp activity at the

human BBB can be induced. Furthermore, because rifampin is also a P-gp substrate and inhibitor (Kim et al., 2002), to prevent it from confounding the interpretation of our data, subjects were instructed to take rifampin nightly so that during the PET imaging study on the following day (~17 hours or ~6 rifampin half-lives after the last rifampin dose), no rifampin was expected to remain in the systemic circulation.

However, the ER (or AUCR, $K1_b$) of ^{11}C-radioactivity in different regions of the brain, in the presence and absence of rifampin treatment, was not significantly different. To account for possible type II error, we computed the 95% CI for ER (and AUCR, $K1_b$) postrifampin treatment versus control. For example, based on ER in brain matter, the CI was 0.59–1.50), thus we can conclude that rifampin does not induce P-gp activity at the human BBB that would result in a decrease in the whole brain ER by more than 41%.

We confirmed that the lack of clinically significant P-gp induction at the human BBB by rifampin was not due to potential confounders such as rifampin-induced increase in verapamil plasma protein binding, changes in verapamil metabolism, or CBF. Additionally, verapamil is an excellent P-gp substrate, its application and validation as a P-gp PET tracer (^{11}C-verapamil) has been extensively studied in several experimental setups (Hendrikse et al., 1998), and its human use was first validated by Sasongko et al. (2005). Although xenobiotic induction of P-gp at the human BBB had never been studied until the present study, others have studied the "induction" of P-gp by epilepsy. Langer et al. (2007) and Bauer et al. (2014) used ^{11}C-verapamil as the PET ligand to detect seizure-induced regional increases in P-gp activity. Thus, ^{11}C-verapamil PET imaging has been able to detect an increase in P-gp activity at the human BBB due to disease and therefore should be able to detect an increase in P-gp activity at the human BBB due to xenobiotic induction.

There are several possible explanations for why the P-gp induction at the human BBB is not clinically significantly (41% decrease in whole-brain ER). First, PXR expression at the human BBB may be too low (or absent) to induce P-gp activity despite sufficient rifampin exposure. The mRNA expression of PXR, constitutive androstane receptor (CAR), and aryl hydrocarbon receptor (AhR) has been previously evaluated in human brain microvessels (isolated from epilepsy patients). Transcripts of PXR or CAR were not detected, but those of AhR were (Dauchy et al., 2008). Second, rifampin concentration achieved within the brain microvessel endothelial cells may not be high enough to induce P-gp. After daily oral rifampin administration, the unbound intestinal plasma rifampin concentrations will be much higher than those in the systemic circulation, and therefore it is not surprising that intestinal P-gp expression and activity are induced by rifampin. Rifampin exposure to the intracellular milieu of the brain endothelial cells will be further reduced by P-gp efflux from these cells. Third, P-gp at the human BBB may already be maximally induced by environmental or endogenous factors. Therefore, further induction may not be possible.

In conclusion, our findings showed that quinidine, at its therapeutic concentrations, inhibits P-gp activity at the human BBB to result in ~60% increase in the brain ER of ^{11}C-verapamil radioactivity, which was greater than the 40% inhibition previously observed with supratherapeutic blood concentrations of CsA (Muzi et al., 2009). However, the magnitudes of inhibition by both drugs make neither drug suitable to deliberately inhibit P-gp at the human BBB to sufficiently enhance CNS delivery of drugs. These findings, as well as our previous findings on the ^{11}C-verapamil–CsA drug interaction at the human BBB, have been echoed by Kalvass et al. (2013). Although the magnitude of quinidine–^{11}C-verapamil DDI was quantitatively predicted by data from the macaque and cells expressing MDR1, additional studies are required to determine the best preclinical species for predicting P-gp–based DDI at the human BBB. Furthermore, our study showed that rifampin is unlikely to induce P-gp at the BBB in a clinically significant manner and produce P-gp drug interactions at the BBB. However, this does not imply that P-gp at the human BBB cannot be induced by xenobiotics or via other P-gp expression regulatory pathways. In addition to PXR, CAR, and AhR, other nuclear receptors such as glucocorticoid or vitamin D receptors have been reported to regulate P-gp expression (Aiba et al., 2005; Reschly et al., 2006; Martin et al., 2008; Miller et al., 2010), thus their expression in the brain endothelial cells should be determined. Drugs that are ligands of these receptors should also be tested to determine if they can clinically significantly induce in vivo P-gp activity at the human BBB.

Acknowledgments

The authors thank Eric Helgeson, Steve Shoner, Xuehi Li, the PET suite staff at the University of Washington Medical Center, and Brian Kirby for their assistance in conducting the PET studies. The authors also thank Mark Muzi for helpful discussions on data analysis.

Authorship Contributions

Participated in research design: Collier, Liu, Unadkat.

Conducted experiments: Collier, Deo, Domino, Eary, Hsiao, Link, Liu, Mankoff, Unadkat.

Contributed new reagents or analytic tools: Link, Liu, Spiekerman.

Performed data analysis: Liu, Spiekerman.

Wrote or contributed to the writing of the manuscript: Collier, Deo, Domino, Link, Mankoff, Liu, Spiekerman, Unadkat.

References

Aiba T, Susa M, Fukumori S, Hashimoto Y (2005) The effects of culture conditions on CYP3A4 and MDR1 mRNA induction by 1alpha,25-dihydroxyvitamin D(3) in human intestinal cell lines, Caco-2 and LS180. *Drug Metab Pharmacokinet* **20**:268–274.

Aller SG, Yu J, Ward A, Weng Y, Chittaboina S, Zhuo R, Harrell PM, Trinh YT, Zhang Q, and Urbatsch IL, et al. (2009) Structure of P-glycoprotein reveals a molecular basis for poly-specific drug binding. *Science* **323**:1718–1722.

Bankstahl JP, Kuntner C, Abrahim A, Karch R, Stanek J, Wanek T, Wadsak W, Kletter K, Müller M, and Löscher W, et al. (2008) Tariquidar-induced P-glycoprotein inhibition at the rat blood-brain barrier studied with (R)-11C-verapamil and PET. *J Nucl Med* **49**:1328–1335.

Bauer B, Yang X, Hartz AM, Olson ER, Zhao R, Kalvass JC, Pollack GM, Miller DS (2006) In vivo activation of human pregnane X receptor tightens the blood-brain barrier to methadone through P-glycoprotein up-regulation. *Mol Pharmacol* **70**:1212–1219.

Bauer M, Karch R, Zeitlinger M (2014) In vivo P-glycoprotein function before and after epilepsy surgery. *Neurology* **83**:1326–1331.

Bauer M, Zeitlinger M, Karch R, Matzneller P, Stanek J, Jäger W, Böhmdorfer M, Wadsak W, Mitterhauser M, and Bankstahl JP, et al. (2012) Pgp-mediated interaction between (R)-[11C] verapamil and tariquidar at the human blood-brain barrier: a comparison with rat data. *Clin Pharmacol Ther* **91**:227–233.

Borst P and Schinkel AH (2013) P-glycoprotein ABCB1: a major player in drug handling by mammals. *J Clin Invest* **123**:4131–4133.

Brunton LL, Blumenthal DK, Murri N, Dandan RH, and Knollmann BC (2011) Goodman & Gilman's The Pharmacological Basis of Therapeutics, *12th ed*, McGraw-Hill, New York, p 855.

Chan G, Saldivia V, Yang Y, Pang H, de Lannoy I, Bendayan R (2013) In vivo induction of P-glycoprotein expression at the mouse blood-brain barrier: an intracerebral microdialysis study. *J Neurochem* **127**:342–352.

Cirrito J.R, Deane R, Fagan AM, Spinner ML, Parsadanian M, Finn MB, Jiang H, Prior JL, Sagare A, Bales KR, Paul SM, Zlokovic BV, Piwnica-Worms D, Holtzman DM (2005) P-glycoprotein deficiency at the blood-brain barrier increases amyloid-beta deposition in an Alzheimer disease mouse model. J Clin Invest **115**:3285–3290.

Dauchy S, Dutheil F, Weaver RJ, Chassoux F, Daumas-Duport C, Couraud PO, Scherrmann J.M, De Waziers I, Declèves X (2008) ABC transporters, cytochromes P450 and their main transcription factors: expression at the human blood-brain barrier. J Neurochem **107**:1518–1528.

Deo AK, Borson S, Link JM, Domino K, Eary JF, Ke B, Richards TL, Mankoff DA, Minoshima S, O'Sullivan F, Eyal S, Hsiao P, Maravilla K, Unadkat JD (2014) Activity of p-glycoprotein, a β-amyloid transporter at the blood-brain barrier, is compromised in patients with mild alzheimer disease. J Nucl Med **55**:1106–1111.

Eyal S, Chung FS, Muzi M, Link JM, Mankoff DA, Kaddoumi A, O'Sullivan F, Hebert MF, and Unadkat JD (2009) Simultaneous PET imaging of P-glycoprotein inhibition in multiple tissues in the pregnant nonhuman primate. *J Nucl Med* **50**:798–806.

Eyal S, Ke B, Muzi M, Link JM, Mankoff DA, Collier AC, and Unadkat JD (2010) Regional P-glycoprotein activity and inhibition at the human blood-brain barrier as imaged by positron emission tomography. *Clin Pharmacol Ther* **87**:579–585.

Frigo GM, Perucca E, Teggia-Droghi M, Gatti G, Mussini A, and Salerno J (1977) Comparison of quinidine plasma concentration curves following oral administration of some short- and long-acting formulations. *Br J Clin Pharmacol* **4**:449–454.

Gurley BJ, Swain A, Williams DK, Barone G, Battu SK (2008) Gauging the clinical significance of P-glycoprotein-mediated herb-drug interactions: comparative effects of St. John's wort, Echinacea, clarithromycin, and rifampin on digoxin pharmacokinetics. *Mol Nutr Food Res* **52**: 772–779.

Hamman MA, Bruce MA, Haehner-Daniels BD, Hall SD (2001) The effect of rifampin administration on the disposition of fexofenadine. *Clin Pharmacol Ther* **69**:114–421.

Hartz AM, Miller DS, Bauer B (2010) Restoring blood-brain barrier P-glycoprotein reduces brain amyloid-beta in a mouse model of Alzheimer's disease. *Mol Pharmacol* **77**:715–723.

Hendrikse NH, Schinkel AH, de Vries EG, Fluks E, Van der Graaf WT, Willemsen A, Vaalburg W, Franssen EJ (1998) Complete in vivo reversal of P-glycoprotein pump function in the blood-brain barrier visualized with positron emission tomography. Br J Pharmacol **124**:1413–1418.

Hsiao P, Bui T, Ho RJ, and Unadkat JD (2008) In vitro-to-in vivo prediction of P-glycoprotein-based drug interactions at the human and rodent blood-brain barrier. *Drug Metab Dispos* **36**: 481–484.

Hsiao P, Sasongko L, Link JM, Mankoff DA, Muzi M, Collier AC, and Unadkat JD (2006) Verapamil P-glycoprotein transport across the rat blood-brain barrier: cyclosporine, a concentration inhibition analysis, and comparison with human data. *J Pharmacol Exp Ther* **317**:704–710.

Hsiao P and Unadkat JD (2014) Predicting the outer boundaries of P-glycoprotein (P-gp)-based drug interactions at the human blood-brain barrier based on rat studies. *Mol Pharm* **11**: 436–444.

Ito K, Uchida Y, Ohtsuki S, Aizawa S, Kawakami H, Katsukura Y, Kamiie J, and Terasaki T (2011) Quantitative membrane protein expression at the blood-brain barrier of adult and younger cynomolgus monkeys. *J Pharm Sci* **100**:3939–3950.

Kaddoumi A, Choi SU, Kinman L, Whittington D, Tsai CC, Ho RJ, Anderson BD, and Unadkat JD (2007) Inhibition of P-glycoprotein activity at the primate blood-brain barrier increases the distribution of nelfinavir into the brain but not into the cerebrospinal fluid. *Drug Metab Dispos* **35**:1459–1462.

Kalvass JC, Polli JW, Bourdet DL, Feng B, Huang SM, Liu X, Smith QR, Zhang LK, and Zamek-Gliszczynski MJ; International Transporter Consortium (2013) Why clinical modulation of efflux transport at the human blood-brain barrier is unlikely: the ITC evidence-based position. *Clin Pharmacol Ther* **94**:80–94.

Kim, RB (2002) Drugs as P-glycoprotein substrates, inhibitors, and inducers. *Drug Metab Rev* **34**: 47–54.

Kreisl WC, Liow JS, Kimura N, Seneca N, Zoghbi SS, Morse CL, Herscovitch P, Pike VW, and Innis RB (2010) P-glycoprotein function at the blood-brain barrier in humans can be quantified with the substrate radiotracer 11C-N-desmethyl-loperamide. *J Nucl Med* **51**:559–566.

Langer O, Bauer M, Hammers A, Karch R, Pataraia E, Koepp MJ, Abrahim A, Luurtsema G, Brunner M, Sunder-Plassmann R, Zimprich F, Joukhadar C, Gentzsch S, Dudczak R, Kletter K, Müller M, Baumgartner C (2007) Pharmacoresistance in epilepsy: a pilot PET study with the P-glycoprotein substrate R-[(11)C]verapamil. *Epilepsia* **48**:1774–1784.

Liow JS, Kreisl W, Zoghbi SS, Lazarova N, Seneca N, Gladding RL, Taku A, Herscovitch P, Pike VW, and Innis RB (2009) P-glycoprotein function at the blood-brain barrier imaged using 11C-N-desmethyl-loperamide in monkeys. *J Nucl Med* **50**:108–115.

Martin C, Berridge G, Higgins CF, Mistry P, Charlton P, and Callaghan R (2000) Communication between multiple drug binding sites on P-glycoprotein. *Mol Pharmacol* **58**:624–632.

Martin P, Riley R, Back DJ, Owen A (2008) Comparison of the induction profile for drug disposition proteins by typical nuclear receptor activators in human hepatic and intestinal cells. Br J Pharmacol **153**:805–819.

Miller DS (2010) Regulation of P-glycoprotein and other ABC drug transporters at the blood-brain barrier. *Trends Pharmacol Sci* **31**:246–254.

Muzi M, Mankoff DA, Link JM, Shoner S, Collier AC, Sasongko L, and Unadkat JD (2009) Imaging of cyclosporine inhibition of P-glycoprotein activity using 11C-verapamil in the brain: studies of healthy humans. *J Nucl Med* **50**:1267–1275.

Narang VS, Fraga C, Kumar N, Shen J, Throm S, Stewart CF, Waters CM (2008) Dexamethasone increases expression and activity of multidrug resistance transporters at the rat blood-brain barrier. *Am J Physiol Cell Physiol* **295**:C440–450.

Niemi M, Backman JT, Fromm MF, Neuvonen PJ, Kivistö KT (2003) Pharmacokinetic interactions with rifampicin : clinical relevance. Clin Pharmacokinet **42**:819–850.

Nussey S and Whitehead S (2001) *Endocrinology: An Integrated Approach*, p 327, BIOS Scientific Publishers, Oxford.

Ott M, Fricker G, Bauer B (2009) Pregnane X receptor (PXR) regulates P-glycoprotein at the blood-brain barrier: functional similarities between pig and human PXR. *J Pharmacol Exp Ther* **329**:141–149.

Passchier J, Comley R, Salinas C, Rabiner E, Gunn R, Cunningham V, Wilson A, Houle S, Gee A, and Laruelle M, (2008) Blood brain barrier permeability of [11C]loperamide in humans under normal and impaired P-glycoprotein function. *J Nucl Med* **49**:211P.

Pauli-Magnus C, von Richter O, Burk O, Ziegler A, Mettang T, Eichelbaum M, and Fromm MF (2000) Characterization of the major metabolites of verapamil as substrates and inhibitors of P-glycoprotein. *J Pharmacol Exp Ther* **293**:376–382.

Reece PA and Peikert M (1980) Simple and selective high-performance liquid chromatographic method for estimating plasma quinidine levels. *J Chromatogr A* **181**:207–217.

Reich T and Rusinek H (1989) Cerebral cortical and white matter reactivity to carbon dioxide. *Stroke* **20**:453–457.

Reschly EJ and Krasowski MD (2006) Evolution and function of the NR1I nuclear hormone receptor subfamily (VDR, PXR, and CAR) with respect to metabolism of xenobiotics and endogenous compounds. *Curr Drug Metab* **7**:349–365.

Sadeque AJ, Wandel C, He H, Shah S, and Wood AJ (2000) Increased drug delivery to the brain by P-glycoprotein inhibition. *Clin Pharmacol Ther* **68**:231–237.

Sasongko L, Link JM, Muzi M, Mankoff DA, Yang X, Collier AC, Shoner SC, and Unadkat JD (2005) Imaging P-glycoprotein transport activity at the human blood-brain barrier with positron emission tomography. *Clin Pharmacol Ther* **77**:503–514.

Schinkel AH, Smit JJ, van Tellingen O, Beijnen JH, Wagenaar E, van Deemter L, Mol CA, van der Valk MA, Robanus-Maandag EC, and te Riele HP, et al. (1994) Disruption of the mouse mdr1a P-glycoprotein gene leads to a deficiency in the blood-brain barrier and to increased sensitivity to drugs. *Cell* **77**:491–502.

Seneca N, Zoghbi SS, Liow JS, Kreisl W, Herscovitch P, Jenko K, Gladding RL, Taku A, Pike VW, and Innis RB (2009) Human brain imaging and radiation dosimetry of 11C-N-desmethyl-loperamide, a PET radiotracer to measure the function of P-glycoprotein. *J Nucl Med* **50**:807–813.

Shawahna R, Uchida Y, Declèves X, Ohtsuki S, Yousif S, Dauchy S, Jacob A, Chassoux F, Daumas-Duport C, and Couraud PO, et al. (2011) Transcriptomic and quantitative proteomic analysis of transporters and drug metabolizing enzymes in freshly isolated human brain microvessels. *Mol Pharm* **8**:1332–1341.

Sun H, Dai H, Shaik N, Elmquist WF (2003) Drug efflux transporters in the CNS. *Adv Drug Deliv Rev* **55**:83–105.

Tracy TS, Korzekwa KR, Gonzalez FJ, and Wainer IW (1999) Cytochrome P450 isoforms involved in metabolism of the enantiomers of verapamil and norverapamil. *Br J Clin Pharmacol* **47**:545–552.

Uchida Y, Ohtsuki S, Katsukura Y, Ikeda C, Suzuki T, Kamiie J, and Terasaki T (2011) Quantitative targeted absolute proteomics of human blood-brain barrier transporters and receptors. *J Neurochem* **117**:333–345.

Unadkat JD, Chung F, Sasongko L, Whittington D, Eyal S, Mankoff D, Collier AC, Muzi M, and Link J (2008) Rapid solid-phase extraction method to quantify [(11)C]-verapamil, and its [(11)C]-metabolites, in human and macaque plasma. *Nucl Med Biol* **35**:911–917.

Vogelgesang S, Cascorbi I, Schroeder E, Pahnke J, Kroemer HK, Siegmund W, Kunert-Keil C, Walker LC, Warzok RW (2002) Deposition of Alzheimer's beta-amyloid is inversely correlated with P-glycoprotein expression in the brains of elderly non-demented humans. *Pharmacogenetics* **12**:535–541.

Yuen N, Anderson SE, Glaser N, Tancredi DJ, and O'Donnell ME (2008) Cerebral blood flow and cerebral edema in rats with diabetic ketoacidosis. *Diabetes* **57**:2588–2594.

Zolnerciks JK, Booth-Genthe CL, Gupta A, Harris J, and Unadkat JD (2011) Substrate- and species-dependent inhibition of P-glycoprotein-mediated transport: implications for predicting in vivo drug interactions. *J Pharm Sci* **100**:3055–3061.

Address correspondence to: Jashvant D. Unadkat, Department of Pharmaceutics, School of Pharmacy, Box 357610, University of Washington, Seattle, WA 98195-7610. E-mail: jash@u.washington.edu